Unexpected Compositional and Structural Modification of CoPt₃ Nanoparticles by Extensive Surface Purification

Martín D. Mizrahi,[a] Galyna Krylova,[b] Lisandro J. Giovanetti,[a] José M. Ramallo-López,[a] Yuzi Liu,[b] Elena V. Shevchenko,[b]* and Félix G. Requejo[a]*

[a]INIFTA, CONICET and Dpto. Química, Facultad de Ciencias Exactas, Universidad Nacional de La Plata, P.O. Box 16, Suc. 4, 1900 La Plata, Buenos Aires, Argentina,

[b]Center for Nanoscale Materials, Argonne National Laboratory, Argonne, Illinois 60439 USA.

Corresponding authors: Elena V. Shevchenko (eshevchenko@anl.gov) and Felix G. Requejo (felix.requejo@gmail.com).

ABSTRACT

We combined synchrotron small angle X-ray scattering, X-ray fluorescence and extended X-ray absorption fine structure spectroscopy to probe the structure of chemically synthesized CoPt₃ nanoparticles (NPs) after ligand removal via the commonly accepted solvent/nonsolvent approach. We showed that improved catalytic activity of extensively purified NPs could not be explained only in terms of a "cleaner" surface. We found that extensive surface purification results in the substantial leaching of the Co atoms from the chemically synthesized CoPt₃ NPs transforming them into CoPt₃/Pt core/shell structures with unexpectantly thick (~0.5 nm) Pt shell. We indicated that the improved catalytic activity of extensively purified NPs in octyne hydrogenation reaction can be explained by the formation of CoPt₃/Pt core/shell structures. Also, we demonstrated that drastic compositional and structural transformation of water transferred CoPt₃ NPs was rather a result of extensive removal of native ligands via solvent/nonsolvent approach than leaching of cobalt atoms in aqueous media. We expect that these findings can be relevant to other transition metal based multicomponent NPs.

1. INTRODUCTION

Multicomponent nanoparticles (NPs) became an important class of materials due to their abilities to carry multiple functions of the individual constituents and to generate novel properties as a result of the interplay between the building blocks.[1-10] They were considered for a broad range of applications such as catalysis,[11-17] magnetic storage systems,[18] biomedicine,[19-24] and fuel cells.[13, 25] In particular, the alloys of

Pt with transition metals were recognized for their exceptional catalytic properties.[13-17] It was found that polycrystalline Pt alloyed with 3d-transition metals was 2-4 times more active than polycrystalline Pt for the electrochemical oxygen reduction.[26] However, the advanced catalytic properties of Pt-based alloy films were often attributed to the formation of Pt-skin,[27-28] that can be obtained by dissolution of non-platinum atoms via acidic treatment or as a result of complete segregation of Pt atoms at the surface during high temperature annealing.[26] Theoretical studies on CoPt clusters based on the Monte Carlo simulations[29-31] and genetic algorithm with a many-body potential[32,33] indeed revealed the preferential segregation of Pt atoms at surface. However, the surface composition of bimetallic NPs under catalytic reaction conditions can be significantly affected by the reactants.

Previous studies demonstrated that the surface of bimetallic NPs can undergo complex transformations upon their exposure to different media.[23, 33-35] For example, experimental studies on 10-12 nm Co-Pt alloy NPs showed the migration of Co atoms and formation of a strained epitaxial CoO film upon their high temperature exposure to oxygen, while in a reducing atmosphere of hydrogen, the Co atoms migrated back to the bulk, leaving a monolayer of platinum atoms on the surface.[35] Similar phenomenon under oxidizing or reducing conditions was observed for Rh-Pd alloy NPs.[33] While in the gaseous environment the compositional transformations were reversible, irreversible leaching of Fe was reported for FePt in aqueous media.[23] Since the NP surface characteristics are critical for their performance as catalysts,[26–28] understanding of the compositional uniformity in such system and its stability is critical for further advancing of the design principles of highly efficient catalytic structures. However, despite the significant progress in synthesis of binary metal alloy NPs, there is still no clear understanding of the correlation between the "bulk" composition and the surface structure.

Easy to scale colloidal synthesis in organic solvents is an attractive way to synthetize highly monodisperse NPs with precisely controlled size, shape, morphology, and overall composition. However, it is capitalized on active use of organic molecules that control the kinetic of the nucleation and growth of NPs. Since these molecules are often expected to passivate the surface in chemical catalysis and negatively affect the conductivity in the NP layers in electrocatalysis, they are usually removed via extensive washing using solvent-nonsolvent approach. As a result, the improved catalytic activity of washed NPs is attributed to the "cleaner" surface of NPs and higher number of the available catalytic sites. Solvent/nonsolvent purification approach is commonly considered to be rather gentle and is expected to allow avoiding the structural transformations of NPs observed in traditional high temperature cleaning procedures.[36-37] However, recently it was shown that certain surface stabilizing ligands can, in fact, significantly improve catalytic selectivity of multicomponent NPs in hydrogenation reactions.[38-41] Therefore the role of surface ligands and the need for "clean" surface are not that unambiguous.

Nevertheless, surface modification with desired functional ligands also involves thorough removal of original molecules via solvent/nonsolvent purification. While interactions of the ligands with the surface of luminescent semiconductor NPs and the impact of their removal on the optical properties are extensively studied,[42-46] in the case of metal NPs the discussion on surface purification is mainly limited to the ligand removal and subsequent formation of clean NPs surface without providing insights into the nature of ligand-surface interactions. In the light of previously reported structural transformations of multicomponent NPs as a result of their exposure to the reactive environment,[7, 23, 33-35] and change of the overall elemental composition observed for semiconductor metal chalcogenide NPs as a result of surface purification,[43] we decided to investigate the effect of NP surface purification by solvent/nonsolven approach on composition and structure of transition metal alloy NPs and its impact on the catalytic properties.

In this work, we focus our study on understanding the effects of the thorough surface purification on the surface composition and structure of bimetallic Pt-based alloy NPs synthetized in organic solvent. Using Transmission Electron Microscopy (TEM), Small Angle X-ray Scattering (SAXS), X-ray fluorescence (XRF) and Extended X-ray Adsorption Fine Structure spectroscopy (EXAFS) we provide a detailed analysis of the structure of chemically synthetized $CoPt_3$ NPs after ligand removal via commonly accepted solvent/nonsolvent approach. We show that extensive solvent/nonsolvent purification applied to 5.9 nm $CoPt_3$ NPs results in the formation of unexpectantly thick (~0.5 nm) Pt shell. We explain the improved catalytic activity of extensively purified NPs in octyne hydrogenation reaction by the formation of $CoPt_3$/Pt core/shell structures via leaching of cobalt atoms from the NP surface. We also demonstrate that the phase transfer of $CoPt_3$ NPs and their prolonged exposure to the water can result in the formation of ~0.7 nm thick Pt shell; however, such thick film was mainly formed as a result of extensive surface purification implemented for effective ligand exchanges and phase transfer. We conclude that purification of the surface of transition-based metal NPs by solvent/nonsolvent can significantly affect their structure and composition. Understanding of this effect is critical for the design of efficient catalysts and surface modification for targeted applications.

2. EXPERIMENTAL SECTION

Chemicals: Platinum acetylacetonate (Pt(acac)$_2$, Acros Organics, 98%); dicobalt octacarbonyl, (Co2(CO)8, stabilized with 1−5% of hexane, Strem); diphenyl ether (DPE, Aldrich, 99%); toluene (Aldrich, 99.5%); ethanol (anhydrous, ASC grade, Pharmaco-Aaper); isopropanol (Fisher Scientific, 99.9%); methanol (Riedel-de Haen, 99.9%); hexadecylamine (HDA, Aldrich, 90%); 1-adamantanecarboxylic acid (ACA, Aldrich, 99%); were used as received without any further purification

Synthesis: The $CoPt_3$ NPs of two different sizes were synthesized according to previously reported protocol.[47] Briefly, $Pt(acac)_2$ (0.033 g) and ACA (0.25 g) were dissolved at 55 °C under nitrogen flow in a mixture of HDA (4 g) and DPE (2 mL). Then 0.043 g of $Co_2(CO)_8$ dissolved in 0.7 mL of DCB were injected into the reaction solution heated up to 170 °C or 145 °C to synthetize ~6 nm or ~9 nm $CoPt_3$ NPs, respectively. The reaction mixture was kept at the temperature of the injection for 1 h. After that NPs were annealed at ~ 246 °C for 15−20 min and the reaction solution was cooled down to 70 °C and 5 mL of chloroform were injected. The NPs were isolated from the unreacted species by precipitation with ethanol (25 mL) followed by centrifugation. The precipitates were re-dispersed in 2-3 mL of toluene or chloroform and filtered through a 0.2 µm PTFE filter. Additional solvent/nonsolvent rounds were applied to remove the excess of stabilizers and byproducts by precipitation with 2-propanol and centrifugation, followed by their dissolution in chloroform. The synthesis of 3.5 nm Pt NPs was conducted according to Ref.[38]

Phase Transfer of NPs: 9.3 nm $CoPt_3$ NPs were transferred into water according to the protocol described in ref.[48-49] The solutions of NPs were washed by multiple washing rounds with alcohols. A mixture of methanol and ethanol was used for the first round while other purification rounds were performed with 2-propanol. The volume ratio of the NPs solution to the nonsolvent was about 1 to 10. Final precipitate was re-dissolved in 1 mL of chloroform, and PEGylated phospholipid (PEG-PE, 1,2-distearoyl-sn-glycero-3-phosphoethanolamine-N-[methoxy(polyethylene glycol)-2000] (ammonium salt), Avanti Polar Lipids) dissolved in chloroform (10 mg/ mL) solution was added. The flask was attached to the Schlenk-line and chloroform was allowed to evaporate under the flow of nitrogen. Next, 10 mL of water were added in which dry precipitate readily re-dispersed upon several seconds of gentle sonication. After that, aqueous solution of NPs (1.5 mL) was placed into the 0.5-3 mL Slide-A-Lyser dialysis cassette with molecular weight 3500 MWCO and dialyzed versus 300 mL of DI water under stirring for 11 days.

Catalytic Studies: The hydrogenation of reaction of 4-octyne was carried out in a stainless steel reactor at room temperature for 15 min under H_2 atmosphere (200 psig). In a standard condition, the reaction solution was prepared by dispersing corresponding NPs in 1.0 mL of dodecane containing 3.75 wt % (255 mM) of 4-octyne.

Characterization:

Transmission electron microscopy (TEM) measurements were performed using a FEI Tecnai F30 microscope operated at 300 kV. TEM samples were prepared by dropping and drying of 1-2 µL of corresponding NP toluene solutions on a carbon-coated copper grid (Ted Pella). Energy Dispersive X-ray

Spectroscopy (EDX) data and dark field STEM and EDX elemental mapping images were obtained using FEI Tecnai F20ST TEM/STEM.

X-ray Absorption Fine Structure (XAFS) experiments were performed at the XAFS-2 beamline at the LNLS (Laboratorio Nacional de Luz Sincrotron), Campinas, Brazil. Extended X-ray Absorption Fine structure (EXAFS) spectra at the Pt L_3-edge (11564 eV) and EXAFS and X-ray Absorption Near Edge Structure (XANES) at the Co K-edge (7709 eV) were recorded at room temperature using a Si (111) crystal monochromator in transmission mode with three ion chambers as detectors. The absorption of the sample was determined between the first two chambers and the third one was used to measure the corresponding metallic reference, placed between the last two chambers, simultaneously with the sample. The EXAFS data were extracted from the measured absorption spectra by standard methods using ATHENA software which was part of the IFFEFIT package.[50] Fourier transformation was calculated using Hanning filtering function and EXAFS modeling was carried out using the ARTEMIS program (IFFEFIT package). Structural parameters (coordination numbers, bond lengths, and their mean squared disorders) were obtained by a nonlinear least-squares fit of the theoretical EXAFS signal to the data in R space by Fourier transforming both the theory and the data. Theoretical scattering path amplitudes and phase shifts for all paths used in the fits were calculated using the FEFF6 code.[51] The k-range was set from 2 to 14 Å^{-1}. The passive reduction factor S_0^2 values were restrained between 0.92 and 0.76 for Pt-L$_3$ and Co-K edges analysis respectively. These values were obtained from the fitting of metallic Pt and Co foils standards by constraining the coordination number in these compounds of known crystal structure. Simultaneously, x-ray fluorescence spectra were taken using a 15-element germanium solid state detector connected to a multichannel analyzer.

Small Angle X-ray Scattering (SAXS) Reciprocal space information was obtained from SAXS experiments performed at the SAXS-2 beamline of the Laboratório Nacional de Luz Síncrotron (LNLS), in Campinas, Brazil. The isotropic SAXS intensity was measured as a function of the scattering vector $q = (4\pi / \lambda)\sin\theta$, λ being the wavelength (λ = 0.161 nm), and 2θ the scattering angle. SAXS curves were normalized to equivalent intensity of the direct x-ray beam and the parasitic scattering from slits was subtracted. Because of the small cross-section of the direct X-ray beam at the detector plane, it was not necessary to correct the SAXS curve for smearing effects. Samples were measured in toluene suspension in a liquid cell with mica disk as windows. SAXS analysis were performed using SASFit software (https://kur.web.psi.ch/sans1/SANSSoft/sasfit.html), using a core/shell form function with a LogNormal size distribution function for the core radii. Details of the form factor function could be found in the software manual. The scattering contrast relative to the matrix (toluene) of the core (CoPt$_3$ alloy) and that

of the shell (Pt) were calculated from the bulk material parameters and were fixed during the fitting procedures.

RESULTS and DISCUSSION.

Phase transfer and chemical stability of CoPt$_3$ NPs: As-synthetized 9.3±0.7 nm CoPt$_3$ NPs (Figure 1) were additionally purified 3 times using solvent/nonsolvent method. This procedure decreased the concentration of organic ligands down to about 4 wt. %.[49] Elemental distribution data shows a rather uniform distribution of Co and Pt atoms across 9.3 nm CoPt$_3$ NP (Figure 1). The Energy Dispersive X-ray Spectroscopy (EDX) results revealed the ratio of Pt to Co as 78 to 22 at. %, that correlates well with the stoichiometric CoPt$_3$ NPs.

In our earlier study,[49] we reported a leaching of Co atoms after a phase transfer of CoPt$_3$ NPs into water. The amount of leached Co (+2) was comparable with the estimated amount of Co atoms at the surface of CoPt$_3$ NPs. Also, a continuous release of Fe atoms in aqueous media was reported for FePt NPs.[23] In order to estimate the impact of ion leaching on the elemental distribution within NPs, we conducted a detailed study on 9.3 nm CoPt$_3$ NP transferred into water using phospholipid block-copolymer micelles [48-49] by applying combined experimental approach that included synchrotron SAXS, XRF, and EXAFS techniques.
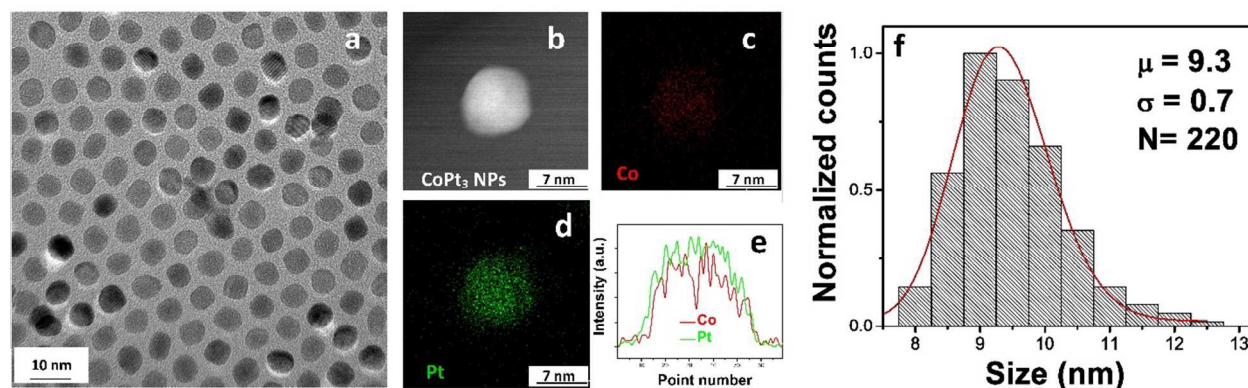

Figure 1. *TEM overview of 9.3 nm CoPt$_3$ NPs (a); dark field STEM image (b) EDX mapping images obtained by acquiring EDX spectra including the Co L series (c) and Pt L series (d); the line-scans derived from elemental maps across 9.3 nm CoPt$_3$ NPs (e); size histograms calculated based on analysis of 220 NPs (f).*

To determine the chemical composition of water transferred 9.3 nm CoPt$_3$ NPs, we performed XRF experiments. Figure 2a shows the experimental XRF spectra obtained using an excitation energy of 11850

eV and corresponding fit performed using PyMca software.[52] Analysis of these fitting data, that took into account the cross section correction for the used excitation energy, allowed to estimate the atomic ratio of Pt to Co as 5.4, value that is significantly higher than the stoichiometric 1 to 3 ratio of $CoPt_3$ alloy.

The elemental distribution in water transferred NPs was analyzed by probing the local structure around Co and Pt atoms by EXAFS that can provide structural information of nanomaterials with both homogeneous and non-homogeneous distribution of elements by the analysis of the fitted averaged coordination numbers.[53] Figure 2b shows the Fourier transforms of the EXAFS oscillations obtained at the Co-K and Pt-L_3 edges as well as the corresponding fitting curves. A model with two coordination shells with Co and Pt atoms as scatters in each shell was used to fit Pt-L_3 EXAFS data, while only one coordination shell of Pt atoms was necessary to fit Co-K edge EXAFS data. The Pt, CoPt[54] and $CoPt_3$[55] bulk alloys were used as references in EXAFS analysis. Table 1 summarizes the structural parameters derived from the EXAFS fits and compares them with the values obtained for corresponding reference samples.
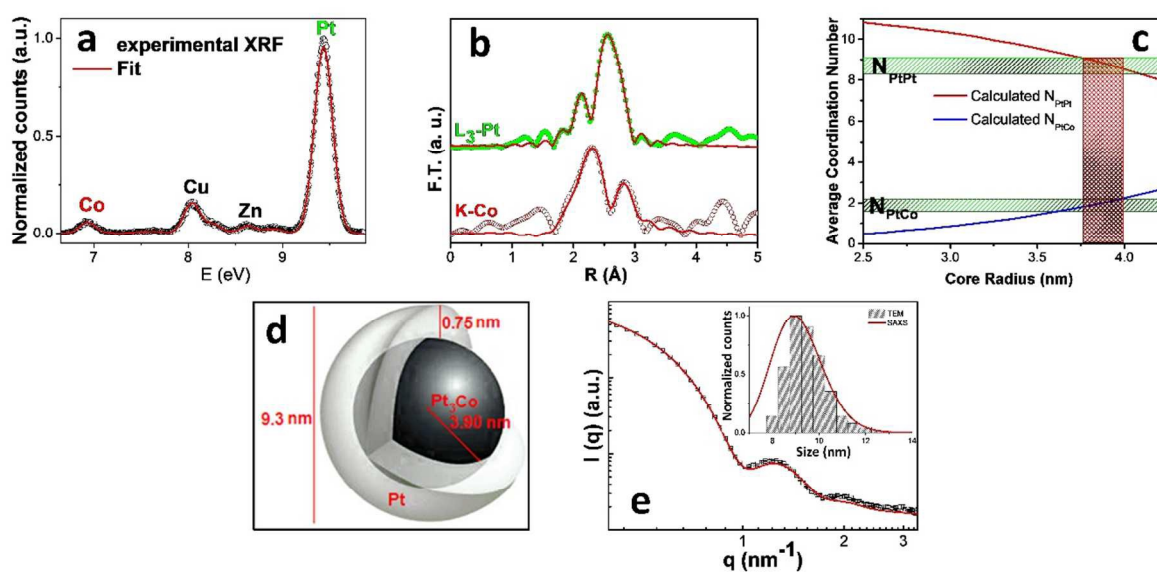

Figure 2. *Summary of the structural characterization for water transferred 9.3 nm $CoPt_3$ NPs. The XRF spectrum (open circles) and its fit (red curve) (a). The Zn and Cu signals belong to the substrate. Fourier transforms of the EXAFS oscillations at the Co-K and Pt- L_3 edges and corresponding fits (red curves) (b). Calculated average coordination numbers, N_{PtPt} (red line) and N_{PtCo} (blue line) as a function of $CoPt_3$ core radius. The green horizontal bars represent the average coordination numbers derived from the EXAFS fits. The vertical red bar indicates range of the $CoPt_3$ core radius that allow obtaining the coordination numbers matching the experimental data. (c). Depiction of the possible core/shell structure (d) reconstructed based on the data shown in (c). SAXS (open symbols) and the fitting curve obtained based on a spherical core/shell model. The size distributions reconstructed from fitting curve was overlapped with the size distribution data obtained based on the TEM data (e, insert).*

The EXAFS results at the Co K-edge revealed the Co-Pt interatomic distance of ~2.72(3) Å that is similar to 2.71, characteristic of the $CoPt_3$ alloy reference. Only a Pt shell was found around Co atoms, that is indicative to $CoPt_3$ structure (Table 1). Fitting of the EXAFS data obtained at Pt L_3-edge also indicated that the Co-Pt interatomic distances are similar to those of $CoPt_3$ alloy. Although we should expect a contraction of Pt-Pt distances[56-58] due to the enhancement of surface tension in NP,[59] the interatomic Pt-Pt distances derived from Pt-L_3 EXAFS fitting curve are greater than those in both $CoPt_3$ and CoPt alloys. Also, the EXAFS fitting data indicated a higher number of the Pt atoms coordinated to other Pt atoms (8.7(4) vs. 8, characteristic to $CoPt_3$ alloy) and lower number of Pt atoms coordinated to Co atoms (1.9(3) vs. 4, characteristic to $CoPt_3$ alloy). However, these results can be explained by the co-existence of bimetallic and metallic phases.

Table 1. *Structural parameters obtained from the EXAFS fits at the Co-K and Pt-L_3 edges for water transferred 9.3 nm and extensively purified 5.9 nm $CoPt_3$ NPs and reference values for bulk Pt and bulk CoPt, and $CoPt_3$ alloys.*

	Co-K					Pt-L_3					
	N_{CoPt}	R_{Co-Pt} (Å)	σ^2_{Co-Pt} (Å^2)	N_{CoCo}	R_{Co-Co} (Å)	N_{PtPt}	R_{Pt-Pt} (Å)	σ^2_{Pt-Pt} (Å^2)	N_{PtCo}	R_{Pt-Co} (Å)	σ^2_{Pt-Co} (Å^2)
Water transferred 9.3 nm $CoPt_3$ NPs	11.4_{10}	2.72_3	0.009_1	-	-	8.7_4	2.74_2	0.007_1	1.9_3	2.70_2	0.009_1
Extensively washed 5.9 nm $CoPt_3$ NPs	10.6_{10}	2.70_3	0.008_1	-	-	8.3_4	2.73_1	0.006_1	1.7_3	2.69_1	0.007_1
Pt	-	-	-	-	-	12	2.77	-	-	-	-
CoPt	8	2.65	-	4	2.69	4	2.69	-	8	2.65	-
CoPt$_3$	12	2.71	-	0	-	8	2.71	-	4	2.71	-

First of all, since the Pt-Pt distances in the bulk Pt and in the $CoPt_3$ alloy are 2.77 and 2.71 Å, respectively, the average value for Pt-Pt distance in the structure with two coexisting metallic phases is consistent with our fitted value of 2.74 Å (Table 1). Note, that the EXAFS results excluded the possibility of the presence of CoPt alloy phase in our samples. The obtained Pt-Co distances and the absence of a Co-Co shell as first neighbors constituted a strong evidence of the $CoPt_3$ alloy as the bimetallic phase. Second, the ratio of coordination numbers for Pt atoms, N_{PtPt}/N_{PtCo}, for water transferred sample was about 4.6, though these ratios for stoichiometric CoPt and $CoPt_3$ alloys are 0.5 and 2, respectively. Such high N_{PtPt}/N_{PtCo} ratio strongly suggests that a fraction of the Pt atoms in NPs, indeed, segregated and

8

formed rather extended domain of Pt.[60] Third, the coordination number of Pt derived from the data obtained at the Co K-edge was around 11, that is consistent with the coordination number for Pt atoms in $CoPt_3$. This means that Co atoms belong to the phase that also contains Pt atoms supporting the presence of bimetallic alloy phase.

In summary, both the interatomic distance and the average coordination numbers obtained from the EXAFS fittings (see Table 1) are consistent with the presence of two Pt-containing phases: metallic Pt and Pt-Co alloy, most likely $CoPt_3$. Since NPs had spherical shape (Figure 1), it was reasonable to assume $CoPt_3$/Pt core/shell structure.

In order to estimate the radius of the alloy core in the water transferred NPs, we calculated the theoretical average coordination numbers N_{PtPt} (Figure 2c, red curve) and N_{PtCo} (Figure 2c, blue curve) for $CoPt_3$/Pt core/shells NPs with different $CoPt_3$ core radii keeping the external radius of NPs fixed to 4.65 nm as it follows from the TEM data (Figure 1). Horizontal green bars represent the average coordination numbers N_{PtPt} and N_{PtCo} determined by the EXAFS experiments. The area of the interception of the green bars and the calculated curves (Figure 2c, red bar) shows that the radius of the $CoPt_3$ core was in the range between 3.8 nm and 4 nm. Hence, the thickness of the Pt shell was around 0.75 nm, that was significantly larger as compared to previous estimation based on the analysis of the concentration of the leached ions.[49] Figure 2d shows the depiction of the possible structure for 9.3 nm water transferred NPs. Based on the core/shell model with ~0.75 nm shell, the ratio of Pt to Co atoms was estimated to be 5.7(6) that is in a good agreement with the ratio of 5.4 calculated based on XRF data (Table 2). It is worth mentioning that the inverse configuration such as Pt/$CoPt_3$ and a random distribution of Pt and Co atoms were also simulated. However, no matching region between the experimental values and the modeled data was found (Figures S1, S2).

Table 2. *Pt to Co atomic ratio obtained based on the analysis of EXAFS and XRF data.*

Samples	EXAFS simulation	XRF
	Pt/Co	Pt/Co
Water transferred 9.3 nm $CoPt_3$ NPs	5.7_6	5.4
Extensively washed 5.9 nm $CoPt_3$ NPs	5.1_4	4.8

To validate the proposed $CoPt_3$/Pt core/shell model, we performed SAXS experiments on the same water transferred NPs that allowed direct determining of the core and shell dimensions. Figure 2e shows the SAXS results and the corresponding fitting data obtained using the spherical form factor and

assuming that the core was CoPt$_3$ alloy and the shell consists of only Pt atoms. As it can be seen in Table 3, the mean core radius and the shell thickness, obtained by SAXS and EXAFS model, are in good agreement. The minor difference of the values obtained from SAXS and EXAFS can be associated with the using of the TEM data in the EXAFS models. While SAXS provide information averaged over the large volume of NPs, TEM was area specific and was limited to the analysis of hundreds of NPs.

The presence of CoPt$_3$ phase in extensively washed CoPt$_3$ NPs was also supported by XANES data (Figure S3). The Co K-edge XANES spectrum revealed the pre-edge feature at 7709 eV and a hump at 7725 eV that correspond to transitions from 1s to 3d and 1s to 4d orbitals in Co atoms, respectively. The positions of the characteristic features and the intensity of the white line of the Co K-edge XANES spectrum extensively washed CoPt$_3$ NPs are nearly the same as those of CoPt$_3$ bulk alloy reference (Figure S3a). In turn, the XANES spectrum of the as–synthesized 9.3 nm CoPt$_3$ NPs was noticeably different, suggesting some differences in the local coordination of the Co atoms in as-synthetized and extensively purified CoPt$_3$ NPs. The Co K-edge EXAFS study on as-synthetized CoPt$_3$ NP indicated the presence of additional coordination shells for Co with Co-Co and Co-O contributions (Figure S3b, Table S1) that is consistent with the presence of oxidized Co atoms at the surface of the as-synthetized NPs.

Combination of the EXAFS and SAXS data strongly supports the core/shell structure of water transferred NPs. Previously, we suggested that cobalt atoms leached only from the surface of CoPt$_3$ NPs based on the analysis of the concentrations of the leached Co (+2) ions to the water by zero background chemiluminesence method.[49] However, chemiluminesence method detected only leached Co (+2) ions after water transfer. In turn, the XRF study on water transferred and dialyzed CoPt$_3$ NPs indicated significantly lower concentration of Co atoms as compared to earlier estimate. Since CoPt$_3$ NPs, that typically underwent 1-3 purification rounds of solvent/nonsolvent treatment, were reported to have elemental composition close to stoichiometric,[47, 49, 61] and the concentration of Co and Pt in 9.3 nm CoPt$_3$ NPs after 3 solvent/nonsolvent rounds and before water transfer was estimated by EDX as 22 and 78 at.%, respectively, it was reasonable to assume that a significant Co depletion of CoPt$_3$ NPs took place as a result of preparation of NP surface for phase transfer such as additional solvent/nonsolvent rounds. Can the surface purification indeed alter the composition of CoPt$_3$ NPs to such extent?

Table 3. *Core radius and shell thickness obtained from SAXS and EXAFS models.*

	SAXS model		EXAFS model	
	Mean core radius, nm	Shell thickness, nm	Mean core radius, nm	Shell thickness, nm

Water transferred 9.3 nm CoPt$_3$ NPs	3.60_5	0.72_1	3.9_1	0.75_{10}
Extensively washed 5.9 nm CoPt$_3$ NPs	2.17_5	0.59_2	2.40_5	0.55_5

Typically, 1-2 purification rounds are applied to as-synthetized NPs that results in preserving of 12-35 wt.% of organic molecules depending on the NP size.[38, 62] However, some applications, such as catalysis or electrocatalysis require cleaner surfaces. High temperature procedures, e.g. calcination[63-64] and extensive surface purification[36, 38] aimed on removal of adsorbed molecules are applied to improve the performance of NPs as catalysts. While in the case of unary NP catalysts the removal of ligands can straightforwardly increase the number of available catalytic sites; however, there is no systematic understanding of the effect of surface purification of the multicomponent NPs on their composition.

Previously, we found that the extensive (4-5 rounds) purification rounds of CoPt$_3$ NPs prevented the formation of CoPt$_3$/Au dumbbells.[7] Since the presence of Co (+2) atoms at the surface of metallic seeds was required for successful synthesis of bimetallic heterostructures with standard gold precursor such as AuCl$_3$, suppression of Au nucleation on the extensively washed CoPt$_3$ seeds pointed out to the possibility of leaching of cobalt atoms from the surface of CoPt$_3$ NPs during solvent/nonsolvent purification rounds.

The leaching of transition metal atoms from the NPs as a result of the surface purification can have a strong effect on the catalytic properties of platinum-transition metal alloy NPs. In order to provide the insights into the effect of the solvent/nonsolvent purification approach on the chemical stability of CoPt$_3$ NPs, we conducted a detailed study on the thoroughly washed catalytically active CoPt$_3$ NPs using the same methodology as we developed for analysis of water transferred NPs.

Effect of solvent-nonsolvent purification of CoPt$_3$ NPs on their catalytic properties: In this study, we used 5.9 nm CoPt$_3$ NPs as a model system. This NP size was selected based on two factors. First of all, smaller sized NPs are expected to reveal a higher catalytic activity as a result of higher total surface area and hence smaller size was more relevant for catalytic studies. Second, we wanted to study the Co depletion in NPs those volume was below the volume corresponding to ~0.7 nm thick Pt shell revealed in the case of 9.3 nm water transferred NPs.

Figure 3 shows the TEM image of ~5.9±0.7 nm CoPt$_3$ NPs synthetized according to the protocols described in Ref.[47, 65] Similar to the case of 9.3 nm CoPt$_3$ NPs, the line-scans derived from elemental maps across individual 5.9 nm CoPt$_3$ NPs after 3 solvent/nonsolvent rounds suggest rather uniform distribution of Co and Pt atoms (Figure 3). According to the EDX analysis, the Pt to Co ratio was 79 to 21

at. % and did not deviate from stoichiometric 3 to 1, characteristic to CoPt$_3$ alloy. The detailed characterization of as-synthetized CoPt$_3$ NPs was provided in numerous previous studies.[47, 61, 65-67]
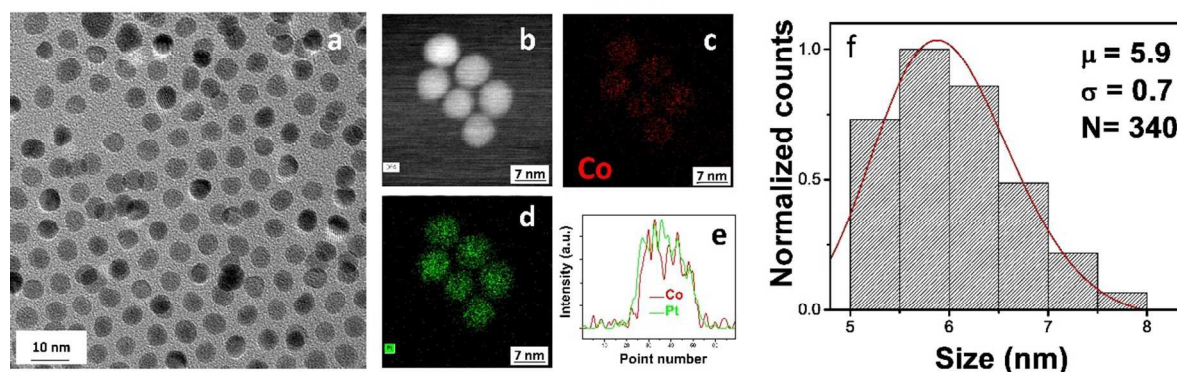

Figure 3. *TEM overview image of 5.9 nm CoPt$_3$ NPs (a); dark field STEM image (b), EDX mapping images obtained by acquiring EDX spectra including the Co L series (c) and Pt L series (d); the line-scans derived from elemental maps across 5.9 nm CoPt$_3$ NPs (e); size histograms calculated based on analysis of 340 NPs (f).*

Octyne hydrogenation was chosen as a model reaction to test the effect of extensive purification of CoPt$_3$ NPs on the catalytic properties. We observed the significant difference in the performance of CoPt$_3$ NPs depending on the number of the purification rounds. For example, 5.9 nm CoPt$_3$ NPs that underwent only three purifications rounds demonstrated a lower activity in hydrogenation reaction of 4-octyne as compared to extensively (5 solvent/nonsolvent rounds) washed NPs. Two additional purification rounds allowed increasing the conversion of 4-octyne from 65 to 86.5% (Figure 4). In principle, this result alone can be explained in terms of the increased number of catalytically active sites at the surface of extensively washed NPs. However, the performance of extensively washed 5.9 nm CoPt$_3$ NPs exceeded even the performance of extensively washed chemically synthetized 3.5 nm Pt NPs that provided higher overall number of catalytic sites. Hence, "cleaner catalytic surface" argument only cannot explain the observed data. Nevertheless, higher catalytic activity of extensively purified 5.9 nm CoPt$_3$ NPs as compared to 3.5 nm Pt NPs can be potentially explained by formation of Pt skin since Pt-based alloys of transition metals with 100% Pt skin were previously reported to overperform Pt.[27-28] However, such structures were previously obtained via dissolution of non-platinum atoms by an acid.[26] Can it be that purification of NP surface using organic solvent/nonsolvent approach results in a drastic compositional and structural change of CoPt$_3$ NPs?
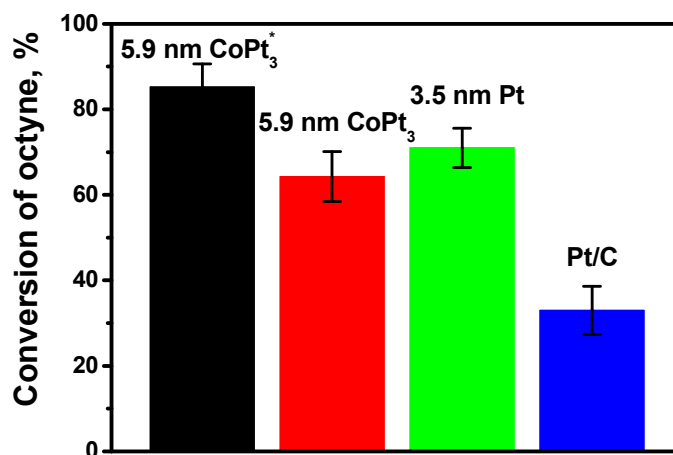
Figure 4. *Summary on catalytic activities of CoPt₃ and Pt NPs and commercially available Pt on carbon (Pt/C sample) in octyne hydrogenation reaction. Two solvent/nonsolvent rounds were applied to 5.9 nm CoPt₃ NPs. The 5.9 nm CoPt₃* and 3.5 nm Pt NPs underwent 5 purification rounds. Prior to catalytic tests, all studied samples were exposed to nitrogen plasma for 1 minute. The same amounts for catalytically active NPs were used in tests. The performance of commercial Pt/C sample is shown for a comparison.*

Similar to the 9.3 nm NPs, the fit of the XRF spectra (Figure 5a) obtained for 5.9 nm CoPt₃ NPs showed a Pt to Co ratio of 4.8, that is, again, significantly higher as compared to stoichiometric ratio of as-synthetized CoPt₃ NPs. This result also suggests the presence of a second Pt rich phase in this sample. Interatomic distances and average coordination numbers calculated from EXAFS data also indicated that CoPt₃/Pt core/shell structure was formed in the case of extensively washed (5 rounds of solvent/nonsolvent) 5.9 nm or 5.9 nm CoPt₃ NPs. The matching of the average coordination numbers N_{PtPt} and N_{PtCo} calculated for CoPt₃/Pt core/shell NPs with different CoPt₃ core radii with the N_{PtPt} and N_{PtCo} obtained from EXAFS data was observed for the core sizes in the range between 2.35 nm and 2.45 nm (Figure 5c). These data mean that Pt shell was formed around CoPt₃ core in the extensively washed 5.9 nm NPs. The atomic ratio of Pt to Co calculated for CoPt₃/Pt core/shell NPs with approximately 0.55 nm thick Pt shell was found to be 5.1(4), that is in a good agreement with the ratio of 4.8 obtained from XRF spectroscopy data.

Fitting of the SAXS data (Figure 5d) using core/shell approximation revealed the core radius and shell thickness consistent with values obtained by modelling of the EXAFS data (Table 3). Thus we can conclude that extensive washing indeed resulted in the Co depletion of 5.9 nm CoPt₃ NPs leading to the formation of CoPt₃/Pt core/shell structure. The thickness of the Pt shell was estimated to be ~0.55 nm

(Figure 5c). The formation of the Pt shell as a result of extensive surface purification also explains the previously reported suppression of the gold overgrowth at the surface of extensively washed $CoPt_3$ seeds.[7]
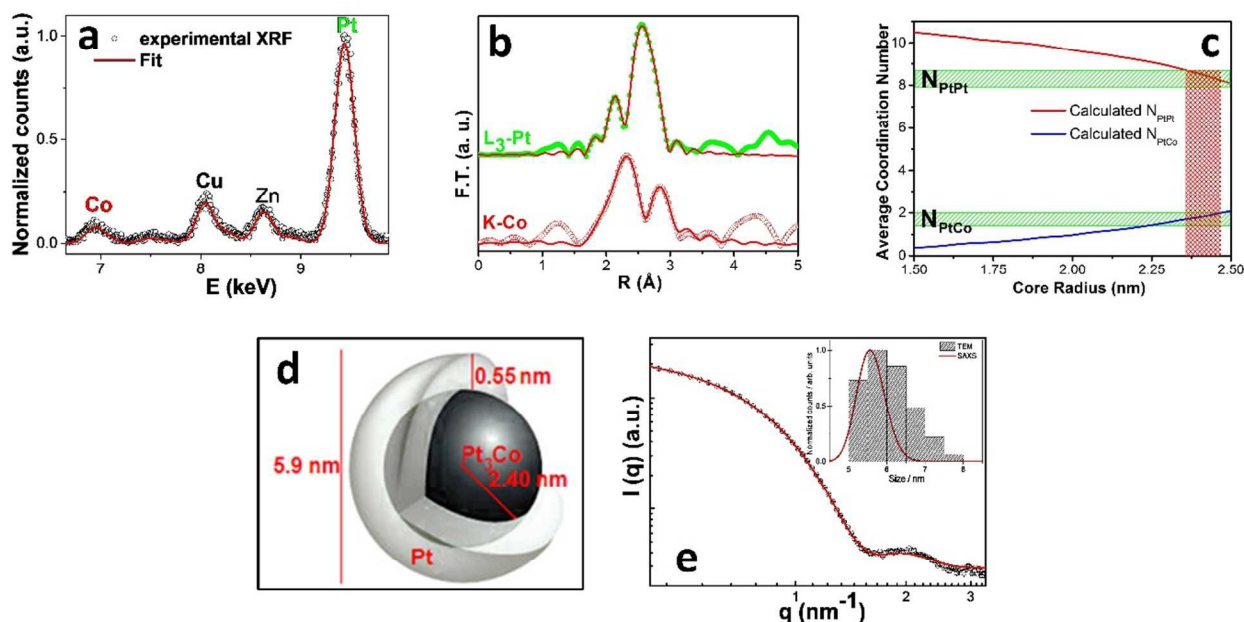
Figure 5. *Summary of the structural characterization for extensively washed 5.9 nm $CoPt_3$ NPs. The XRF spectrum (open circles) and its fit (red curve) (a). The Zn and Cu signals belong to the substrate. Fourier transforms of the EXAFS oscillations at the Co-K and Pt- L_3 edges and corresponding fits (red curves) (b). Calculated average coordination numbers, N_{PtPt} (red line) and N_{PtCo} (blue line) as a function of $CoPt_3$ core radius. The green horizontal bars represent the average coordination numbers derived from the EXAFS fits. The vertical red bar indicates range of the $CoPt_3$ core radius that allow obtaining the coordination numbers matching the experimental data (c). Depiction of the possible core/shell structure (d) reconstructed based on the data shown in (c). SAXS (open symbols) and the fitting curve obtained based on a spherical core/shell model. The size distributions reconstructed from fitting curve was overlapped with the size distribution data obtained based on the TEM data (e, insert).*

CONCLUSIONS

Combination of XRF, EXAFS, and SAXS techniques constitutes a powerful set of chemically selective techniques sensitive to local order that enables investigation of nano- and sub-nanometric structures. Combined use of these techniques reveals the substantial leaching of the Co atoms from chemically synthetized NPs as a result of extensive solvent/nonsolvent purification. This process transforms $CoPt_3$ NPs into $CoPt_3$/Pt core/shell structures with ~0.5 nm thick Pt shell. Therefore Co atoms can leach not only from the surface of NPs as we previously anticipated,[7] but also from the deep inner layers of NPs. The advanced catalytic activity of extensively washed alloy NPs in 4-octyne hydrogenation reaction is explained by the formation of $CoPt_3$/Pt core/shell NPs. Also, the formation of Pt shell explains the suppression of $CoPt_3$/Au dumbbells formation when extensively washed alloy NPs were used as

seeds.[7] Understanding of modification of chemical composition during processing of NPs is critical for our ability to design advanced highly performing heterostructures. Interestingly, the ratio of shell thickness to the radius of the core is found to be 0.21(2) for both 5.9 and 9.3 nm alloy samples; however, the conclusion about the correlation between the Pt shell thickness and the size of the alloy NPs seems to be premature and further studies on differently sized alloy NPs are required.

We limited our study to the chemical stability of the inorganic part since alloy NPs are mainly used in catalysis and electrocatalysis, applications that traditionally require "clean" surface. In turn, other studies, conducted mainly on semiconductor NPs focus on the probing of the organic molecules at the NP surface since proper surface passivation was required for good optical properties.[42, 44-46, 68-71] Nevertheless, irreversible compositional modification of CdSe NPs was observed as a result of removal of surface-bound ligands causing the change of the Cd/Se ratio from 1.1 to 1.0, that in turn, resulted in the decrease of the photoluminescence quantum yield.[43] Also, it was shown for CdSe/ZnS core/shell NPs[44] that initial 2 solvent/nonsolvent purification rounds left a mixture of anionic X-type and two-electron donors L-type ligands and the NP surfaces, while further purification allowed remaining of mainly L-type ligands.[43] Our data are in qualitative agreement with the previous studies on semiconductor NPs; however, we report more significant change in the NP stoichiometry. Thus, we demonstrated that 5.9 nm and 9.3 nm $CoPt_3$ NPs were transformed into core/shell NPs with approximately $CoPt_6$ and $CoPt_9$ compositions, respectively. The understanding of the chemical stability of multicomponent NPs requires further studies on both their inorganic and organic constituents since the nature of capping ligands, solvent and nonsolvent can be all contributing factors. While here we presented study on $CoPt_3$ NPs, similar effects are very likely to be observed for other transition metal based NPs. The preferential leaching of certain elements controlled by solvent/nonsolvent approach can potentially be a promising way to adjust the properties of multicomponent, transition metal based NPs for desired applications.

ACKNOWLEDGMENTS

CONFLICT OF INTERESTS

Nanoscale Accepted Manuscript

The authors declare no competing financial interests.

SUPPORTING INFORMATION

Data on simulated inverse configuration such as Pt/CoPt$_3$ and a random distribution of Pt and Co atoms. Co K-edge XANES analysis of samples and Co reference compounds.
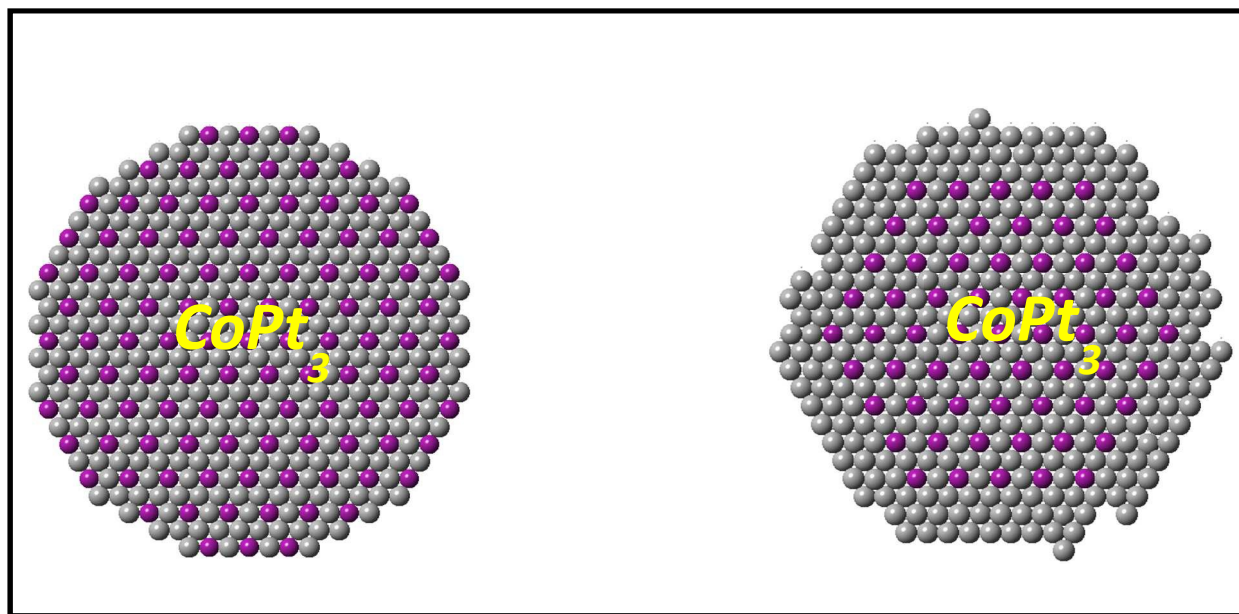
REFERENCES

1.   Li, Y.; Zhang, Q.; Nurmikko, A. V.; Sun, S., Enhanced Magnetooptical Response in Dumbbell-like Ag–CoFe2O4 Nanoparticle Pairs. *Nano Letters* **2005,** *5* (9), 1689-1692.

2.   Bodnarchuk, M. I.; Kovalenko, M. V.; Groiss, H.; Resel, R.; Reissner, M.; Hesser, G.; Lechner, R. T.; Steiner, W.; Schäffler, F.; Heiss, W., Exchange-Coupled Bimagnetic Wüstite/Metal Ferrite Core/Shell Nanocrystals: Size, Shape, and Compositional Control. *Small* **2009,** *5* (20), 2247-2252.

3.   Lim, B.; Kobayashi, H.; Yu, T.; Wang, J.; Kim, M. J.; Li, Z.-Y.; Rycenga, M.; Xia, Y., Synthesis of Pd–Au Bimetallic Nanocrystals via Controlled Overgrowth. *Journal of the American Chemical Society* **2010,** *132* (8), 2506-2507.

4.   Shevchenko, E. V.; Bodnarchuk, M. I.; Kovalenko, M. V.; Talapin, D. V.; Smith, R. K.; Aloni, S.; Heiss, W.; Alivisatos, A. P., Gold/Iron Oxide Core/Hollow-Shell Nanoparticles. *Adv. Mat.* **2008,** *20*, 4323-4329.

5.   Lee, J.-S.; Bodnarchuk, M. I.; Shevchenko, E. V.; Talapin, D. V., "Magnet-in-the-Semiconductor" FePt–PbS and FePt–PbSe Nanostructures: Magnetic Properties, Charge Transport, and Magnetoresistance. *Journal of the American Chemical Society* **2010,** *132* (18), 6382-6391.

6.   Wang, D.; Li, Y., One-Pot Protocol for Au-Based Hybrid Magnetic Nanostructures via a Noble-Metal-Induced Reduction Process. *Journal of the American Chemical Society* **2010,** *132* (18), 6280-6281.

7.   Krylova, G.; Giovanetti, L. J.; Requejo, F. G.; Dimitrijevic, N. M.; Prakapenka, A.; Shevchenko, E. V., Study of Nucleation and Growth Mechanism of the Metallic Nanodumbbells. *Journal of the American Chemical Society* **2012,** *134* (9), 4384-4392.

8.   Costi, R.; Saunders, A. E.; Banin, U., Colloidal Hybrid Nanostructures: A New Type of Functional Materials. *Angewandte Chemie International Edition* **2010,** *49* (29), 4878-4897.

9.   Cozzoli, P. D., Pellegrino, T., Manna, L. , Synthesis, properties and perspectives of hybrid nanocrystal structures. . *Chem. Soc. Rev.* **2006,** *35*, 1195-1208.

10.   Casavola, M.; Falqui, A.; García, M. A.; García-Hernández, M.; Giannini, C.; Cingolani, R.; Cozzoli, P. D., Exchange-Coupled Bimagnetic Cobalt/Iron Oxide Branched Nanocrystal Heterostructures. *Nano Letters* **2009,** *9* (1), 366-376.

11.   Li, X.; Wan, W.; Kattel, S.; Chen, J. G.; Wang, T., Selective hydrogenation of biomass-derived 2(5H)-furanone over Pt-Ni and Pt-Co bimetallic catalysts: From model surfaces to supported catalysts. *Journal of Catalysis* **2016,** *344* (Supplement C), 148-156.

Nanoscale Accepted Manuscript

Nanoscale Accepted Manuscript

12.   Gehl, B.; Flege, J. I.; Aleksandrovic, V.; Schmidt, T.; Kornowski, A.; Bernstorff, S.; Falta, J.; Weller, H.; Bäumer, M., Plasma modification of CoPt3 nanoparticle arrays: A route to catalytic coatings of surfaces. *Journal of Vacuum Science & Technology A: Vacuum, Surfaces, and Films* **2008,** *26* (4), 908-912.

13.   Jiang, L.-Y.; Lin, X.-X.; Wang, A.-J.; Yuan, J.; Feng, J.-J.; Li, X.-S., Facile solvothermal synthesis of monodisperse Pt2.6Co1 nanoflowers with enhanced electrocatalytic activity towards oxygen reduction and hydrogen evolution reactions. *Electrochimica Acta* **2017,** *225* (Supplement C), 525-532.

14.   Li, Q.; Wu, L.; Wu, G.; Su, D.; Lv, H.; Zhang, S.; Zhu, W.; Casimir, A.; Zhu, H.; Mendoza-Garcia, A.; Sun, S., New Approach to Fully Ordered fct-FePt Nanoparticles for Much Enhanced Electrocatalysis in Acid. *Nano Letters* **2015,** *15* (4), 2468-2473.

15.   Guo, S.; Li, D.; Zhu, H.; Zhang, S.; Markovic, N. M.; Stamenkovic, V. R.; Sun, S., FePt and CoPt Nanowires as Efficient Catalysts for the Oxygen Reduction Reaction. *Angewandte Chemie International Edition* **2013,** *52* (12), 3465-3468.

16.   Liu, J.; Xia, T.; Wang, S.; Yang, G.; Dong, B.; Wang, C.; Ma, Q.; Sun, Y.; Wang, R., Oriented-assembly of hollow FePt nanochains with tunable catalytic and magnetic properties. *Nanoscale* **2016,** *8* (22), 11432-11440.

17.   Wang, Y.; Yang, H., Synthesis of CoPt Nanorods in Ionic Liquids. *Journal of the American Chemical Society* **2005,** *127* (15), 5316-5317.

18.   Wu, L.; Mendoza-Garcia, A.; Li, Q.; Sun, S., Organic Phase Syntheses of Magnetic Nanoparticles and Their Applications. *Chemical Reviews* **2016,** *116* (18), 10473-10512.

19.   Pankhurst, Q. A.; Thanh, N. T. K.; Jones, S. K.; Dobson, J., Progress in applications of magnetic nanoparticles in biomedicine. *Journal of Physics D: Applied Physics* **2009,** *42* (22), 224001.

20.   Liu, W.; Naydenov, B.; Chakrabortty, S.; Wuensch, B.; Hübner, K.; Ritz, S.; Cölfen, H.; Barth, H.; Koynov, K.; Qi, H.; Leiter, R.; Reuter, R.; Wrachtrup, J.; Boldt, F.; Scheuer, J.; Kaiser, U.; Sison, M.; Lasser, T.; Tinnefeld, P.; Jelezko, F.; Walther, P.; Wu, Y.; Weil, T., Fluorescent Nanodiamond–Gold Hybrid Particles for Multimodal Optical and Electron Microscopy Cellular Imaging. *Nano Letters* **2016,** *16* (10), 6236-6244.

21.   Ho, D.; Sun, X.; Sun, S., Monodisperse Magnetic Nanoparticles for Theranostic Applications. *Accounts of Chemical Research* **2011,** *44* (10), 875-882.

22.   Chou, S.-W.; Shau, Y.-H.; Wu, P.-C.; Yang, Y.-S.; Shieh, D.-B.; Chen, C.-C., In Vitro and in Vivo Studies of FePt Nanoparticles for Dual Modal CT/MRI Molecular Imaging. *Journal of the American Chemical Society* **2010,** *132* (38), 13270-13278.

23.   Xu, C.; Yuan, Z.; Kohler, N.; Kim, J.; Chung, M. A.; Sun, S., FePt Nanoparticles as an Fe Reservoir for Controlled Fe Release and Tumor Inhibition. *Journal of the American Chemical Society* **2009,** *131* (42), 15346-15351.

24.   Hoskins, C.; Min, Y.; Gueorguieva, M.; McDougall, C.; Volovick, A.; Prentice, P.; Wang, Z.; Melzer, A.; Cuschieri, A.; Wang, L., Hybrid gold-iron oxide nanoparticles as a multifunctional platform for biomedical application. *Journal of Nanobiotechnology* **2012,** *10* (1), 27.

25.   Cui, C.-H.; Yu, S.-H., Engineering Interface and Surface of Noble Metal Nanoparticle Nanotubes toward Enhanced Catalytic Activity for Fuel Cell Applications. *Accounts of Chemical Research* **2013,** *46* (7), 1427-1437.

26.   Stamenkovic, V. R.; Mun, B. S.; Mayrhofer, K. J. J.; Ross, P. N.; Markovic, N. M., Effect of Surface Composition on Electronic Structure, Stability, and Electrocatalytic Properties of Pt-Transition Metal Alloys: Pt-Skin versus Pt-Skeleton Surfaces. *Journal of the American Chemical Society* **2006,** *128* (27), 8813-8819.

27.   van der Vliet, D. F.; Wang, C.; Li, D.; Paulikas, A. P.; Greeley, J.; Rankin, R. B.; Strmcnik, D.; Tripkovic, D.; Markovic, N. M.; Stamenkovic, V. R., Unique Electrochemical Adsorption Properties of Pt-Skin Surfaces. *Angewandte Chemie* **2012,** *124* (13), 3193-3196.

28.   Wang, C.; Markovic, N. M.; Stamenkovic, V. R., Advanced Platinum Alloy Electrocatalysts for the Oxygen Reduction Reaction. *ACS Catalysis* **2012,** *2* (5), 891-898.

29.   Qin, L.; Zhang, Y.; Huang, S.; Tian, H.; Wang, P., Atomic-scale structure of Co-Pt bimetallic nanoparticles: Monte Carlo simulations. *Physical Review B* **2010,** *82* (7), 075413.

30.   Calvo, F.; Mottet, C., Order-disorder transition in Co-Pt nanoparticles: Coexistence, transition states, and finite-size effects. *Physical Review B* **2011,** *84* (3), 035409.

31.   Chepulskii, R. V.; Butler, W. H., Tuning of $L1_{0}$ atomic order in Co-Pt nanoparticles: Ab initio insights. *Physical Review B* **2012,** *86* (15), 155401.

32.   Lu, Q. L.; Zhu, L. Z.; Ma, L.; Wang, G. H., Magnetic properties of Co/Cu and Co/Pt bimetallic clusters. *Chemical Physics Letters* **2005,** *407* (1), 176-179.

33.   Tao, F.; Grass, M. E.; Zhang, Y.; Butcher, D. R.; Renzas, J. R.; Liu, Z.; Chung, J. Y.; Mun, B. S.; Salmeron, M.; Somorjai, G. A., Reaction-Driven Restructuring of Rh-Pd and Pt-Pd Core-Shell Nanoparticles. *Science* **2008,** *322* (5903), 932-934.

34.   Carenco, S.; Tuxen, A.; Chintapalli, M.; Pach, E.; Escudero, C.; Ewers, T. D.; Jiang, P.; Borondics, F.; Thornton, G.; Alivisatos, A. P.; Bluhm, H.; Guo, J.; Salmeron, M., Dealloying of Cobalt from CuCo Nanoparticles under Syngas Exposure. *The Journal of Physical Chemistry C* **2013,** *117* (12), 6259-6266.

35.   Xin, H. L.; Alayoglu, S.; Tao, R.; Genc, A.; Wang, C.-M.; Kovarik, L.; Stach, E. A.; Wang, L.-W.; Salmeron, M.; Somorjai, G. A.; Zheng, H., Revealing the Atomic Restructuring of Pt–Co Nanoparticles. *Nano Letters* **2014,** *14* (6), 3203-3207.

36.   Li, D.; Wang, C.; Tripkovic, D.; Sun, S.; Markovic, N. M.; Stamenkovic, V. R., Surfactant Removal for Colloidal Nanoparticles from Solution Synthesis: The Effect on Catalytic Performance. *ACS Catalysis* **2012,** *2* (7), 1358-1362.

37.   Bonifacio, C. S.; Carenco, S.; Wu, C. H.; House, S. D.; Bluhm, H.; Yang, J. C., Thermal Stability of Core–Shell Nanoparticles: A Combined in Situ Study by XPS and TEM. *Chemistry of Materials* **2015,** *27* (20), 6960-6968.

38.   Kwon, S. G.; Krylova, G.; Sumer, A.; Schwartz, M. M.; Bunel, E. E.; Marshall, C. L.; Chattopadhyay, S.; Lee, B.; Jellinek, J.; Shevchenko, E. V., Capping Ligands as Selectivity Switchers in Hydrogenation Reactions. *Nano Letters* **2012,** *12* (10), 5382-5388.

39.   Binghui Wu, N. Z., Surface and interface control of noble metal nanocrystals for catalytic and electrocatalytic applications. *Nano Today* **2013,** *8* (2), 168-197.

40.   Chen, G.; Xu, C.; Huang, X.; Ye, J.; Gu, L.; Li, G.; Tang, Z.; Wu, B.; Yang, H.; Zhao, Z.; Zhou, Z.; Fu, G.; Zheng, N., Interfacial electronic effects control the reaction selectivity of platinum catalysts. *Nature Materials* **2016,** *15*, 564.

41.   Zhao, Y.; Fu, G.; Zheng, N., Shaping the selectivity in heterogeneous hydrogenation by using molecular modification strategies: Experiment and theory. *Catalysis Today* **2017,** *279*, 36-44.

42.   Anderson, N. C.; Owen, J. S., Soluble, Chloride-Terminated CdSe Nanocrystals: Ligand Exchange Monitored by 1H and 31P NMR Spectroscopy. *Chemistry of Materials* **2013,** *25* (1), 69-76.

43.   Anderson, N. C.; Hendricks, M. P.; Choi, J. J.; Owen, J. S., Ligand Exchange and the Stoichiometry of Metal Chalcogenide Nanocrystals: Spectroscopic Observation of Facile Metal-Carboxylate Displacement and Binding. *Journal of the American Chemical Society* **2013,** *135* (49), 18536-18548.

44.   Zeng, B.; Palui, G.; Zhang, C.; Zhan, N.; Wang, W.; Ji, X.; Chen, B.; Mattoussi, H., Characterization of the Ligand Capping of Hydrophobic CdSe–ZnS Quantum Dots Using NMR Spectroscopy. *Chemistry of Materials* **2017**.

45.   Morris-Cohen, A. J.; Donakowski, M. D.; Knowles, K. E.; Weiss, E. A., The Effect of a Common Purification Procedure on the Chemical Composition of the Surfaces of CdSe Quantum Dots Synthesized with Trioctylphosphine Oxide. *The Journal of Physical Chemistry C* **2010,** *114* (2), 897-906.

46.   Morris-Cohen, A. J.; Malicki, M.; Peterson, M. D.; Slavin, J. W. J.; Weiss, E. A., Chemical, Structural, and Quantitative Analysis of the Ligand Shells of Colloidal Quantum Dots. *Chemistry of Materials* **2013,** *25* (8), 1155-1165.

47.   Shevchenko, E. V.; Talapin, D. V.; Schnablegger, H.; Kornowski, A.; Festin, Ö.; Svedlindh, P.; Haase, M.; Weller, H., Study of Nucleation and Growth in the Organometallic Synthesis of Magnetic Alloy Nanocrystals: The Role of Nucleation Rate in Size Control of CoPt3 Nanocrystals. *Journal of the American Chemical Society* **2003,** *125* (30), 9090-9101.

48.   Dubertret, B.; Skourides, P.; Norris, D. J.; Noireaux, V.; Brivanlou, A. H.; Libchaber, A., In Vivo Imaging of Quantum Dots Encapsulated in Phospholipid Micelles. *Science* **2002,** *298* (5599), 1759-1762.

49.   Krylova, G.; Dimitrijevic, N. M.; Talapin, D. V.; Guest, J. R.; Borchert, H.; Lobo, A.; Rajh, T.; Shevchenko, E. V., Probing the Surface of Transition-Metal Nanocrystals by Chemiluminesence. *Journal of the American Chemical Society* **2010,** *132* (26), 9102-9110.

50.   Ravel, B.; Newville, M., ATHENA, ARTEMIS, HEPHAESTUS: data analysis for X-ray absorption spectroscopy using IFEFFIT. *Journal of Synchrotron Radiation* **2005,** *12* (4), 537-541.

51.   Zabinsky, S. I.; Rehr, J. J.; Ankudinov, A.; Albers, R. C.; Eller, M. J., Multiple-scattering calculations of x-ray-absorption spectra. *Physical Review B* **1995,** *52* (4), 2995-3009.

52.   Solé, V. A.; Papillon, E.; Cotte, M.; Walter, P.; Susini, J., A multiplatform code for the analysis of energy-dispersive X-ray fluorescence spectra. *Spectrochimica Acta Part B: Atomic Spectroscopy* **2007,** *62* (1), 63-68.

53.   Frenkel, A. I.; Yevick, A.; Cooper, C.; Vasic, R., Modeling the Structure and Composition of Nanoparticles by Extended X-Ray Absorption Fine-Structure Spectroscopy. *Annual Review of Analytical Chemistry* **2011,** *4* (1), 23-39.

54.   Leroux, C.; Cadeville, M. C.; Pierron-Bohnes, V.; Inden, G.; Hinz, F., Comparative investigation of structural and transport properties of L1 0 NiPt and CoPt phases; the role of magnetism. *Journal of Physics F: Metal Physics* **1988,** *18* (9), 2033.

55.   Geisler, A. H.; Martin, D. L., A New Superlattice in Co-Pt Alloys. *Journal of Applied Physics* **1952,** *23* (3), 375-375.

56.   Wijnen, P. W. J. G.; Van Zon, F. B. M.; Koningsberger, D. C., Determination of metal particle size in partly reduced Ni catalysts by hydrogen/oxygen chemisorption and EXAFS. *Journal of Catalysis* **1988,** *114* (2), 463-468.

57.   Purdum, H.; Montano, P. A.; Shenoy, G. K.; Morrison, T., Extended-x-ray-absorption-fine-structure study of small Fe molecules isolated in solid neon. *Physical Review B* **1982,** *25* (7), 4412-4417.

58.   Nepijko, S. A.; Pippel, E.; Woltersdorf, J., Dependence of lattice parameter on particle size. *physica status solidi (a)* **1980,** *61* (2), 469-475.

59.   Vermaak, J. S.; Mays, C. W.; Kuhlmann-Wilsdorf, D., On surface stress and surface tension: I. Theoretical considerations. *Surface Science* **1968,** *12* (2), 128-133.

60.   Frenkel, A., *Zeitschrift für Kristallographie - New Crystal Structures* **2007,** *222*, 605-611.

61.   Pellegrino, T.; Fiore, A.; Carlino, E.; Giannini, C.; Cozzoli, P. D.; Ciccarella, G.; Respaud, M.; Palmirotta, L.; Cingolani, R.; Manna, L., Heterodimers Based on CoPt3–Au Nanocrystals with Tunable Domain Size. *Journal of the American Chemical Society* **2006,** *128* (20), 6690-6698.

62.   Ong, W.-L.; Rupich, S. M.; Talapin, D. V.; McGaughey, A. J. H.; Malen, J. A., Surface chemistry mediates thermal transport in three-dimensional nanocrystal arrays. *Nature Materials* **2013,** *12*, 410.

63.   Rioux, R. M.; Song, H.; Hoefelmeyer, J. D.; Yang, P.; Somorjai, G. A., High-Surface-Area Catalyst Design: Synthesis, Characterization, and Reaction Studies of Platinum Nanoparticles in Mesoporous SBA-15 Silica. *The Journal of Physical Chemistry B* **2005,** *109* (6), 2192-2202.

64.   Kim, J.; Lee, Y.; Sun, S., Structurally Ordered FePt Nanoparticles and Their Enhanced Catalysis for Oxygen Reduction Reaction. *Journal of the American Chemical Society* **2010,** *132* (14), 4996-4997.

65.   Shevchenko, E. V.; Talapin, D. V.; Rogach, A. L.; Kornowski, A.; Haase, M.; Weller, H., Colloidal Synthesis and Self-Assembly of CoPt3 Nanocrystals. *Journal of the American Chemical Society* **2002,** *124* (38), 11480-11485.

66.   Kwon, S. G.; Krylova, G.; Phillips, P. J.; Klie, R. F.; Chattopadhyay, S.; Shibata, T.; Bunel, E. E.; Liu, Y.; Prakapenka, V. B.; Lee, B.; Shevchenko, E. V., Heterogeneous nucleation and shape transformation of multicomponent metallic nanostructures. *Nature Materials* **2014,** *14*, 215.

67.   Borchert, H.; Shevchenko, E. V.; Robert, A.; Mekis, I.; Kornowski, A.; Grübel, G.; Weller, H., Determination of Nanocrystal Sizes: A Comparison of TEM, SAXS, and XRD Studies of Highly Monodisperse CoPt3 Particles. *Langmuir* **2005,** *21* (5), 1931-1936.

68.   Knittel, F.; Gravel, E.; Cassette, E.; Pons, T.; Pillon, F.; Dubertret, B.; Doris, E., On the Characterization of the Surface Chemistry of Quantum Dots. *Nano Letters* **2013,** *13* (11), 5075-5078.

69.   Gomes, R.; Hassinen, A.; Szczygiel, A.; Zhao, Q.; Vantomme, A.; Martins, J. C.; Hens, Z., Binding of Phosphonic Acids to CdSe Quantum Dots: A Solution NMR Study. *The Journal of Physical Chemistry Letters* **2011,** *2* (3), 145-152.

70.   Hens, Z.; Martins, J. C., A Solution NMR Toolbox for Characterizing the Surface Chemistry of Colloidal Nanocrystals. *Chemistry of Materials* **2013,** *25* (8), 1211-1221.

71.   Son, J. G.; Choi, E.; Piao, Y.; Han, S. W.; Lee, T. G., Probing organic ligands and their binding schemes on nanocrystals by mass spectrometric and FT-IR spectroscopic imaging. *Nanoscale* **2016,** *8* (8), 4573-4578.

GRAPHYCAL ABSTRACT

HIGHLIGHT

Extensive surface purification of alloy NPs can significantly change their composition and transform them into core/shell nanostructures with the improved catalytic properties.